

Turbulent drag reduction in dam-break flows

Imre M. Jánosi, Dominique Jan, K. Gábor Szabó, Tamás Tél

Abstract The role of turbulence is investigated in dam-break flows, where a finite volume of fluid is released from a compartment into a long, rectangular channel. After a sudden removal of the lock gate, a gravity current, undular bore, or solitary wave develops, depending on the ambient fluid height in the channel. The temporal evolution of the moving front has been measured and evaluated. It was observed that the dilution using a very small amount (a few weight ppm) of a long chain polymer (polyethylene-oxide) in the fluid strongly affected flow properties. Pronounced drag reduction has been found in dry bed flows (whereas the polymer increased the viscosity of the fluid). The presence of a few mm-thick ambient fluid layer in the channel effectively destroyed drag reduction, in spite of the fact that strong turbulence was obvious and the propagation velocity of the front was almost unchanged.

1 Introduction

Since Toms (1949), turbulent drag reduction has attracted considerable attention from both fundamental and practical viewpoints (Lumley 1969; Berman 1978; Bushnell 1991; Gyr and Bewersdorff 1995). In spite of this long history, the exact mechanism responsible for polymer drag reduction is not well understood. The main difficulty is clearly finding the coupling of turbulence and polymer dynamics. Recently, promising attempts by means of effective theories (Sreenivasan and White 2000; Stone et al. 2002; Boffetta et al. 2003a, 2003b; L'vov et al. 2003; Benzi et al. 2004) and direct numerical simulations (Housiadas and Beris 2003; Min et al. 2003a, 2003b; Ptasinski et al. 2003; De Angelis et al. 2003) reproduce important aspects

of dilute polymer dynamics, such as the onset of drag reduction, suppressed wall-normal fluctuations, the logarithmic velocity law, and the maximum drag reduction asymptote (Virk 1975).

In the overwhelming majority of experimental and model studies, the flow has been confined in a cylindrical pipe, plane-wall bounded channel, or a Taylor-Couette setup, and almost exclusively stationary situations have been considered. To the best of our knowledge, the only experiment on polymeric drag reduction in transient flow was performed by Paireau and Bonn (1999). Unsteady situations, however, can help us to better understand important aspects such as the onset phenomenon (Sreenivasan and White 2000) and potential practical applications (Gyr and Bewersdorff 1995) required to explore transient flow regimes as well.

Here, we report on experiments on “dam-break” flows, where a transient current is generated by an instantaneous release of fluid from a lock into a long rectangular channel. Apart from engineering relevance, the idealized problem itself has long been a test case for approximate analytic and numerical solutions (Sturm 2001). Furthermore, this arrangement represents the limit of extreme density-difference gravity currents (Simpson 1997), where two fluids of non-equal densities are allowed to adjust as a barrier initially separating them is suddenly removed. Intermediate density ratios can be realized by using dense gases (Gröbelbauer et al. 1993). The analogy is complete for the dry bed case of dam-break flow (no ambient liquid layer in the channel), where the thinner fluid is the ambient air.

In this work, we demonstrate that the presence of a dilute polymer influences primarily dry bed flows; modifying effects of the polymer additive disappear when there is an ambient layer in the channel. The experimental setup and the dam-break flow features in clean water are presented in Sect. 2. Our results are summarized in Sect. 3. Detailed analysis of the initial flow phases fully supports the conclusion obtained by Cadot et al. (1998): drag reduction occurs only if turbulence is forced by a smooth boundary layer, and the phenomenon vanishes in inertially forced turbulent flows. The last section (Sect. 4) is devoted to discussion. Our results provide also a new test bed for studying how far non-Newtonian fluid properties affect the solution of shallow water equations.

2 Basic experiments

The schematic arrangement of our experimental tank is shown in Fig. 1. The bottom and side walls are constructed

Received: 23 November 2003 / Accepted: 25 February 2004
Published online: 15 April 2004
© Springer-Verlag 2004

I. M. Jánosi (✉), D. Jan, T. Tél
von Kármán Laboratory for Environmental Flows, Eötvös University,
PO Box 32, 1518, Budapest, Hungary
E-mail: janosi@lecco.elte.hu

K. G. Szabó
HAS Research Group, Institute for Theoretical Physics,
Eötvös University, Pázmány P. sétány 1,
1117 Budapest, Hungary

This work was supported by the Hungarian Science Foundation (OTKA) under Grant Nos. T032423, T032437, and TS044839. The authors are thankful to Gyözö Láng for his assistance in physical-chemical measurements.

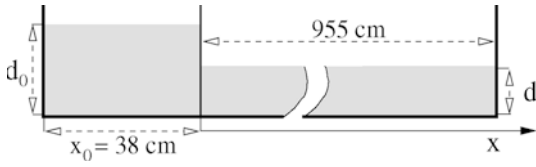


Fig. 1. Schematic arrangement and geometric dimensions of our dam-break experiments

from optically smooth glass, the lock and lock gate are made from Plexiglas. The distance of the lock gate was fixed at $x_0=38$ cm in the experiments presented here and the initial filling height in the lock was varied in the range, $11 \leq d_0 \leq 25$ cm. Coordinate x refers to the position of the moving front of the gravity current, where the origin is fixed at the location of the lock gate. Another key parameter is the ambient fluid depth, d , in the channel.

The experiments were recorded by two CCD cameras: a fast-shutter camera (Sensicam, PCO Imaging) was fixed, which provided the side or plan views (see Figs. 2 and 14) and another small portable camcorder (Sony DCR-PC115E) was fixed on a trolley that was moved along the tank, following the front. The position of the water front as a function of time was determined from digitalized pictures.

Without going into the details, three characteristic temporal regimes can be identified for our dam-break flow. First, there is a short *accelerated regime* caused by the pressure field of the initial condition (the larger fluid level in the lock). Note that the “classical” formulation of the problem assumes an infinite reservoir ($x_0 = \infty$, see Fig. 1). Since the fluid height quickly drops in a short lock, the flow converges to an *inertial regime* after a few sec-

onds. The third phase is a *viscous regime*, dominated by strong skin friction and pronounced contact line instabilities; we will discuss the related points later. The motion of the fluid layer ceases when the kinetic energy has been fully dissipated.

To clearly demonstrate the effects of polymer additive in dam-break flow, we first give a short summary of our observations for the basic phenomena with clean water.

2.1

Dry bed, $d=0$

When fluid is released into a dry channel, the characteristic shape of the front builds up quickly and the acceleration ceases after 0.3–0.5 s. In general, we did not see signs of strong turbulence (Fig. 2a). However, since the Reynolds number is rather large ($Re \sim 3\text{--}4 \times 10^4$, depending on d_0), there must be a turbulent boundary layer at the solid-liquid contact surface. The common definition of Reynolds number for such a current is $Re = Uh/\nu$, where U is the speed, h is a characteristic height behind the front, and ν is the kinematic viscosity of the fluid.

2.2

Shallow ambient layer

In the presence of a continuous fluid layer in the channel, the behavior of the flow becomes remarkably different, even when the ambient depth, d , is only a few mm. A propagating bore develops immediately after removing the lock gate. However, the static layer at the bottom resists to a quick replacement. As a consequence, a “mushroom-like” unstable configuration forms where surface wave breaking occurs in both (forward and reverse) directions. The “mushroom” jet was first reported by Stansby et al.

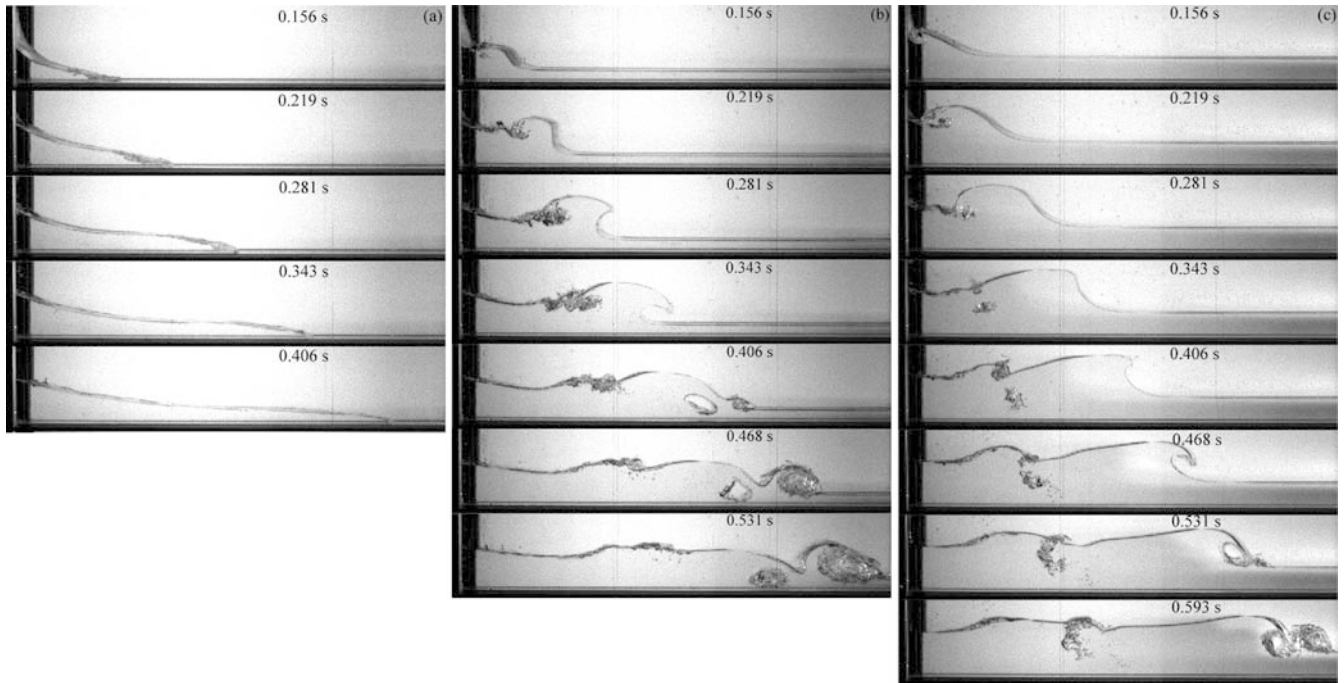


Fig. 2. Sequences of snapshots (66×11 cm²) after releasing fresh water from the lock in the dam-break experiment. $d_0=15$ cm and the ambient fluid depth in front of the lock is a $d=0$ (dry bed), b $d=18$ mm, c $d=38$ mm

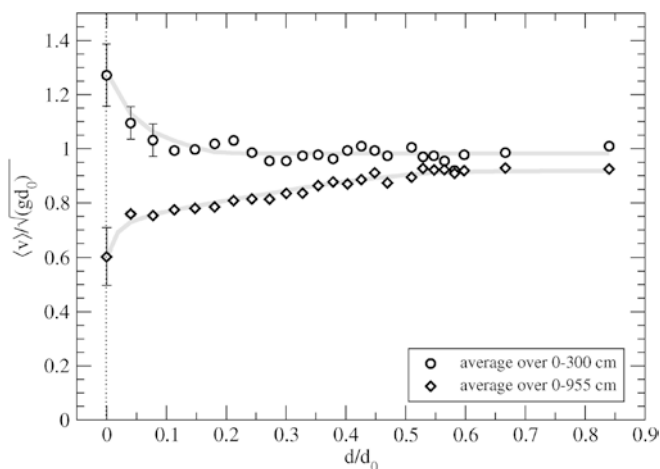


Fig. 3. Average velocity, $\langle v \rangle \equiv x/t$, of the dam-break front at different distances from the point of release vs the height, d , of the ambient, fresh water layer. The velocity is practically height-independent above a certain value of d , where $\langle v \rangle \approx \sqrt{gd_0}$. There is some deviation from this rule close to the dry bed limit, due to the strong skin friction characterizing this case

(1998). Figure 2b shows that the flow is essentially two-dimensional; the effect of side walls is negligible. Wave breaking results in the trapping of air bubbles, which enhances turbulent mixing around the propagating front. The kinetic energy is usually enough to build up a second, third, and sometimes a fourth breaking event until a smooth propagating bore-like perturbation forms (this late stage is not visible in Fig. 2b).

2.3 Deep ambient layer

When the ambient fluid depth, d , is gradually increased in the channel, the properties of the flow change continuously, see Fig. 2c. Interestingly, backward breaking occurs approximately at the same time, but the first forward breaking is delayed proportionally with d . The second instability is weakened until it completely disappears. Bubble trapping remains pronounced. In the limiting case of $d \leq d_0$, a smooth, isolated (but not necessarily symmetric) wave packet forms at the beginning, which is spontaneously transformed into a propagating soliton, as the most robust final stage.

2.4 Propagation velocity

As a first quantitative attribute, the average velocity, $\langle v \rangle$, of the front was determined at different water depths, d , in the channel. The results are shown in Fig. 3. The average velocity, $\langle v \rangle$, was computed over two fixed intervals, [0, 3] m (circles) and [0, 9.55] m (diamonds) by measuring the time of passing.

The first observation is that the average velocity is almost independent of the water level in the channel if d exceeds a value of 15 mm (note that $d_0=15$ cm in this series of experiments). This result is consistent with theoretical predictions (Klemp et al. 1997) and even numerical values agree well. Recall that our reservoir size is far from infinite, thus, we do not expect to reproduce the value, $v_c = 2\sqrt{gd_0}$, of the “canonical” solution (Ritter

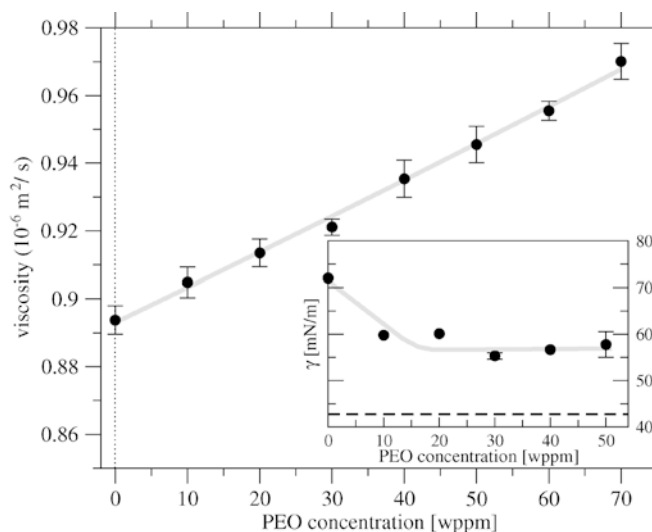


Fig. 4. Material properties of PEO solutions at rest. The kinematic viscosity (measured by the Höppler method) increases with the concentration, while the surface tension (*inset*) drops quickly and saturates. The *dashed line* indicates the surface tension of 8.6 l (a typical lock filling) of distilled water with two drops of the commercial detergent, Dawn

1892). Deviations are more pronounced with dry bed runs; the initial propagation is much faster, but later, skin friction efficiently brakes the flow, resulting in low average values over larger intervals. As the ambient fluid depth is increased, the differences gradually disappear.

3 Experiments with PEO additive

3.1 PEO solution

High concentration ($c=2000$ wppm) stock solution of polyethylene-oxide (PEO) was prepared from dry granules (Aldrich, nominal molecular mass 4×10^6 amu) by solving the proper quantity in distilled water. The liquid was kept on a magnetic stirrer (at the lowest stirring rate) for at least 12 hours to promote complete dissolution. The desired concentration for our flow experiments was set by further dilution prior to filling the lock.

Control measurements were performed on the basic physical properties of low-concentration PEO solutions. Figure 4 illustrates the behavior of kinematic viscosity and surface tension. Viscosity was measured by the standard Höppler method (falling ball viscosimeter) and error bars were obtained from repeated tests at the same concentrations. The viscosity was found to have increased by 5–10% in the concentration range of most of our experiments.

Surface tension was obtained by the differential capillary rise method, a drop of $\sim 20\%$ with respect to clean water was also indicated by an increased foaming at vigorous manipulations. Since surfactants are also known as drag reducing agents (Gyr and Bewersdorff 1995), control measurements were performed with the commercial detergent Dawn (Procter & Gamble); the appropriate value of surface tension is also indicated in Fig. 4 inset.

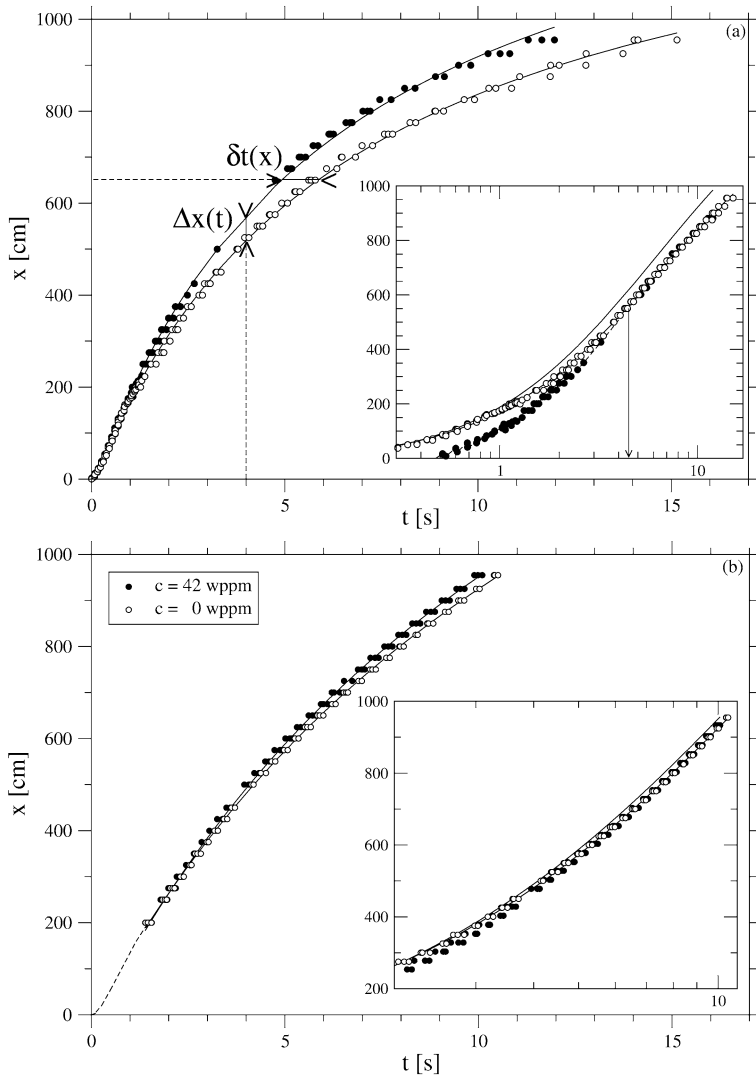


Fig. 5a, b. Displacement of the dam-break front (a) on dry bed, and (b) in a shallow ambient layer of depth $d=5$ mm with (solid circles) and without (open circles) PEO additive. $d_0=15$ cm for both cases. The solid lines are empirical fits, see Eq. 1. The difference between the two fluid motions is characterized by either the displacement difference, $\Delta x(t)$, taken at time t , or the time difference, $\delta t(x)$, between the two flows needed to reach the same distance, x , as indicated in a. The insets (on semi-logarithmic scales) show that the late stage of the flow is identical for clean water and the PEO solutions (see text)

Density changes are negligible in the given concentration range. Preparation and experiments were performed in an air-conditioned laboratory and the air and liquid temperature remained in the range $22\pm 2^\circ$ C. The temperature was permanently monitored throughout the project, but we did not observe any effect that could be associated with temperature anomalies.

3.2 Front propagation

Figure 5 illustrates the effect of PEO on dam-break flow, where the position of the front is shown as a function of time. Good reproduction is demonstrated by the fact that three series are plotted for both the clean and PEO-polluted cases. Pronounced differences are observed for the dry bed runs; the same were hardly measurable for a thin ambient layer where $d=5$ mm (see Fig. 5b). Note that the PEO concentration in the channel was the same as in the lock at each of the wet bed experiments. No detectable differences were found for higher ambient levels.

Quantitative inequalities between the two curves of propagation in Fig. 5a can be evaluated by considering equal time and equal distance differences, $\Delta x(t)$ and $\delta t(x)$,

respectively. This requires interpolation of data because discrete samples (snapshots) cannot have the same parameters for different experimental runs. For large enough times, the curves can be fitted well by using the rational form (also known as the Padé approximation),

$$f(t) = \frac{a_1 + a_2 t}{1 + a_3 t}, \quad (1)$$

with the empirical coefficients a_1 , a_2 , and a_3 . Note that this function has correct asymptotic behavior, since $x(t \rightarrow \infty) = a_2/a_3$, that is, the front stops eventually. The initial value, $x(t=0)=0$, is not expected to be reproduced by $a_1=0$, because the simple form of Eq. 1 cannot fit the accelerating regime.

The general behavior is clear in Fig. 5a: the front propagates faster in the presence of PEO than in the case of clean water. However, the inset illustrates that the late stage ($t \geq 4-5$ s for $d_0=15$ cm, as indicated by the arrow) asymptotics of the flow is independent of the PEO content. In Fig. 5a inset, the data for the PEO solution (solid circles) is shifted vertically (the original position is indicated by the thin solid line). The effect of PEO is almost negligible when the front runs over a fluid film (Fig. 5b).

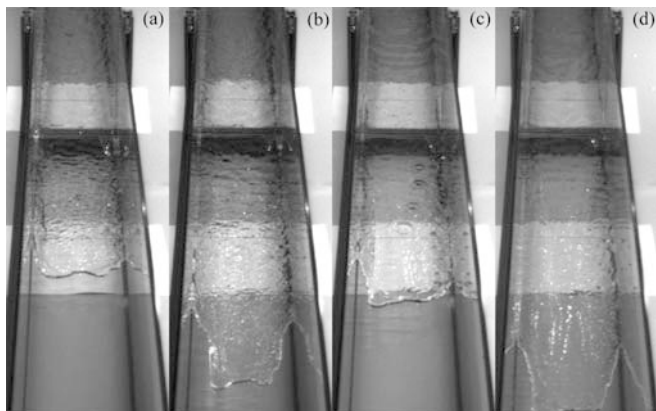


Fig. 6a–d. Perspective view of dry bed fronts shortly after release with $d_0=15$ cm. a Pure water, $t=0.63$ s. b Pure water, $t=0.80$ s. c PEO 42 wppm, $t=0.63$ s. d PEO 42 wppm, $t=0.80$ s. The PEO solution is already faster at this early stage. The texture of the fluid’s surface is different in the two cases: the PEO solution’s surface is not only rough but has elongated structures too. The presence of strong turbulence is perceptibly better from this view than in Fig. 2a

This behavior is expected because it is well known that drag reduction *requires* the flow to *exceed* an “onset Reynolds number”, Re_{dr} , depending on polymer concentration, polymer properties (flexibility, chain length, chemical composition), the type of solvent, and the geometry of the flow (Gyr and Bewersdorff 1995). The comparison of displacement curves gave the estimate, $U \approx 1$ m/s, when the average height of the flow at about one third of the channel is $h \approx 8\text{--}10$ mm, from which we obtained the drag reduction onset Reynolds number in dam-break flows as $Re_{dr} \approx 800\text{--}1100$.

We emphasize that the effect is quantitatively reproducible to the extent illustrated in Fig. 5; the problems of quantitative evaluation are analyzed in the next subsection. Care must be taken to dry the tank completely before a dry bed run because even isolated drops on the bottom decrease the effect considerably.

3.3

Contact line fingering

The main source of errors in reconstructing propagation curves (Fig. 5a) in dry bed experiments is a pronounced fingering instability of the contact line. The

basic phenomena have been known for a long time but they are subjects of intense recent research as well (Kondic 2003). This instability occurs only at the solid-liquid interface; no similar fingering is present when the front moves over a fluid layer.

Figure 6 shows snapshots recorded by the fast-shutter camera from a tilted position above the channel. The first 2 m of the tank is visible. The temporal evolution of the contact line could be reconstructed from the digitalized images by means of a standard affine transformation for linear perspective (Brannan et al. 1999); representative results are shown in Fig. 7. Qualitatively, the contact line is more or less straight and is stable up to a distance of ~ 120 cm. The first distortions appear at the side walls due to the effect of excess braking. The resulting “tongue” suffers from subsequent ramification, and develops two or three fingers. The length and position of the fingers are not steady; rearrangements occur throughout the flow up to the far end of the channel.

Figure 7 includes data on a control experiment (middle frame), where the effect of decreased surface tension was tested. A few drops of the detergent, Dawn (Procter & Gamble), added to the water in the lock (8.6 l) almost halved the surface tension of clean water (see Fig. 4 inset). As for the propagation properties, we did not observe any measurable difference between the clean and the detergent-contaminated water in our dam-break experiments. Lowered surface tension, however, enhanced the tendency towards fingering (Fig. 7). On the other hand, surface tension is not the only parameter determining fingering instability. The PEO additive efficiently decreased skin friction, thus, the initial tongue appeared later and the fingering tendency was also weaker. Eventually, the flow slows down to below a critical velocity (or the onset Reynolds number Re_{dr}), thus, the fingers at the late stage are very similar for clean, detergent or PEO-added water. Nevertheless, the fingers are the main source of inaccurate position and velocity measurements, especially because of the shape of advancing front dynamically changes (see Fig. 7). (Side views permit us to determine the position of the foremost finger’s tip only.)

3.4

Dependence on PEO concentration

Turbulent drag reduction is determined routinely as a function of additive concentration. Two kinds of

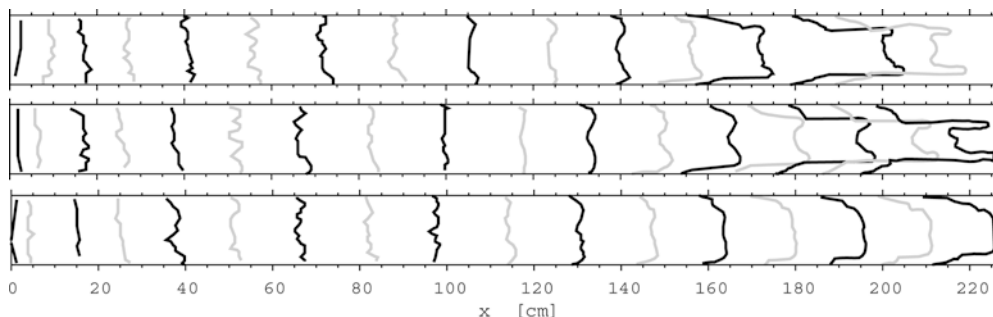


Fig. 7. Time evolution of the front in dry bed experiments. The interval between black and gray contours is 0.12 s, $d_0=15$ cm for each case. *Uppermost frame*: pure water. *Middle frame*: pure water with detergent. *Lower frame*: 42 wppm PEO solution. (In

the *uppermost frame*, the last black and the last but one gray contours are missing. Since the camera was not synchronized to the opening of the lock gate, the contours do not represent equivalent time instants for the three experiments shown.)

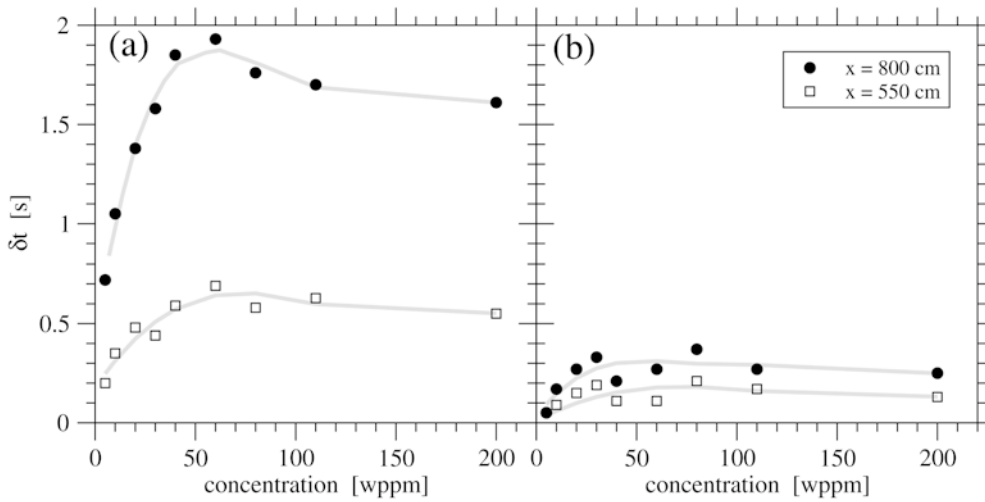


Fig. 8a, b. Time difference, δt , at two distances (see Fig. 5a) as a function of PEO concentration in (a) dry bed and (b) in a shallow ambient layer, $d=5$ mm ($d_0=17$ cm)

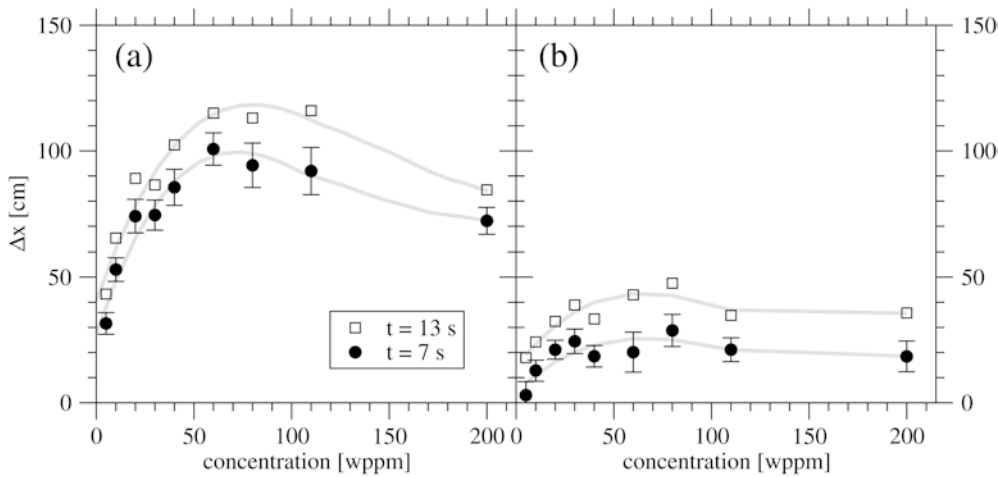


Fig. 9a, b. Displacement difference, Δx (see Fig. 5a), as a function of PEO concentration for two different times in (a) dry bed runs and (b) in $d=5$ mm fluid layers ($d_0=17$ cm). The maximum values are around 70 wppm concentration, just like in the case of Fig. 8

characteristic behavior are experienced, depending on the setup and chemical composition (Gyr and Bewersdorff 1995). In most pipe flow and rotating disk experiments, drag reduction efficiency has a sharp maximum around a concentration of 40–50 wppm, while others report on a sharp increase and a subsequent saturation as a function of PEO concentration. A proper comparison is certainly encumbered by the fact that the sole characteristic provided by PEO producers is the average molecular weight, but nothing more is known about the real distribution of chain length or mass.

Figures 8 and 9 show our results. Equal time differences are evaluated for two parameter sets, one is around the middle and another is close to the end of an experimental run. In general, the differences increase up to a given time or distance and then the values saturate. At higher PEO concentrations, the differences tend to decrease after passing a maximum. A plausible explanation may be based on the fact that drag reduction is a threshold phenomenon; when the Reynolds number drops below Re_{dr} , the reducing effect of the polymer disappears. The resulting slow flow, however, dissipates kinetic energy faster as a consequence of elevated viscosity (see Fig. 4). The analogous phenomena in stationary pipe flows have been measured in great detail by Gampert and Wagner (1984).

The common way to report on a decreased turbulent drag is to give the “percent drag reduction”, $DR(\%)$ (Gyr and Bewersdorff 1995). There are several definitions in use for this quantity, all of which are based on dimensionless ratios of directly measurable variables, which are often indirectly related to friction. For example, a definition based on a specific pressure drop decrease while maintaining the same velocity is quite plausible in a stationary pipe flow experiment (Gyr and Bewersdorff 1995). The situation is not so simple in our case, since the flow is essentially a transient phenomenon. Nevertheless, we can attempt to determine a given $DR(\%)$ value along the same lines by evaluating maximum differences. For example, the maximum time difference for equal distances (see Fig. 5a) is around $\delta t=2$ s at 8 m (see Fig. 8a). As we mentioned, this difference does not grow further. The typical arrival time at 8 m is around $t=9$ s for clean water fronts (see Fig. 5a), thus, we can give an estimate $DR_{\delta t}(\%) = \delta t/t \approx 22\%$. If we do the same for equal time differences ($\Delta x \approx 1$ m at $t=7$ s, the typical distance for clean water flow at the same time is $x=7$ m, see Figs. 9 and 5a), we get $DR_{\Delta x}(\%) = \Delta x/x \approx 14\%$. This clearly illustrates that the value of $DR(\%)$ is tightly bound to the physical quantity on which its definition is based upon.

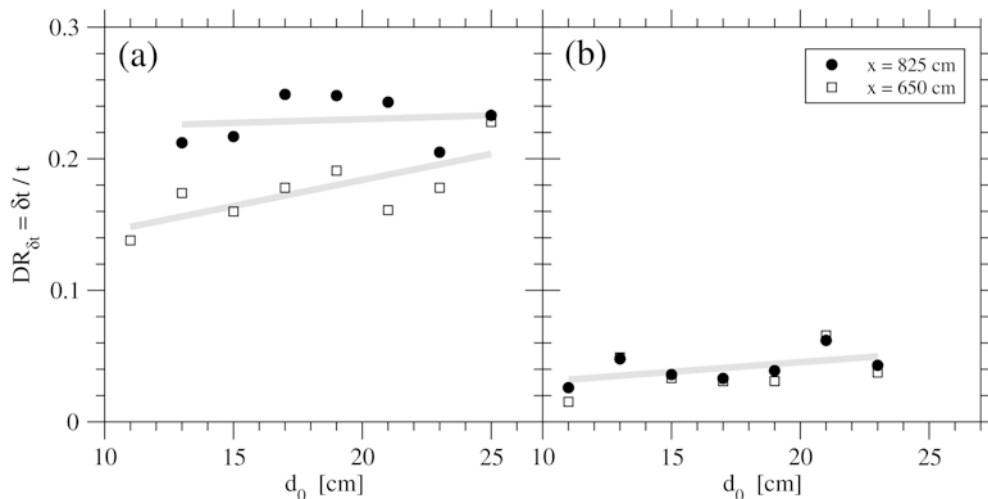


Fig. 10a, b. Normalized time difference, $\delta t/t_{cw}$, at two distances as a function of release height in the lock, d_0 , in (a) dry bed and (b) in a shallow ambient layer, $d=5$ mm ($c=42$ wppm)

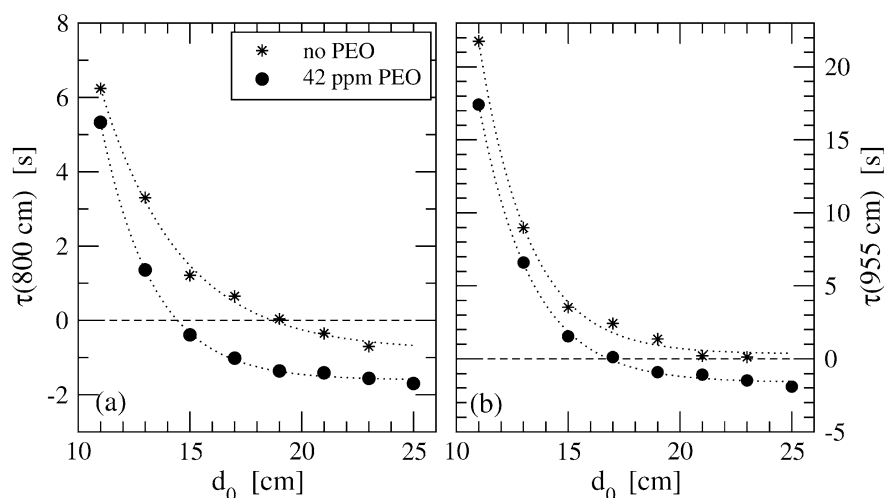


Fig. 11a, b. Arrival time difference, $\tau(x)=t_0(x)-t_{5mm}(x)$, for pure water (stars) and for PEO solution (circles) as a function of release height, d_0 , (a) at a distance of $x=800$ cm and (b) at the end of the tank, $x=955$ cm. Dotted lines indicate exponential fits

3.5 Dependence on lock filling, d_0

The second most important control parameter of the experiments is the fluid level, d_0 , in the lock. The higher its value, the larger the initial potential energy in the system. In the following experimental series, the PEO concentration is fixed at $c=42$ wppm, which is somewhat below the maxima observed in Figs. 8a and 9a, but the viscosity is closer to clean water.

The evaluation of time difference, $\delta t(x)$, at fixed distance, x , as a function of filling height, d_0 , again resulted in remarkable magnitudes for dry bed runs. The general trend is a decrease at higher d_0 , however, the flow itself is much faster at higher initial fluid levels. Therefore, we show in Fig. 10 the normalized difference, $\delta t(x)/t_{cw}(x)$, for the same fixed distances (the index cw refers to clean water value). The trend is slightly increasing for the early flow phase, but there is no dependence on filling height, d_0 , when we compare late stage data.

Another aspect is depicted in Fig. 11 to compare dry bed and shallow ambient layer runs. Here, the arrival time difference is plotted for fixed distances. A negative sign means that the dry bed flow passes the given distance faster. The crossover is more obvious for $x=8$ m

(Fig. 11a) than at the end of the tank (Fig. 11b). This result is consistent with the qualitative picture again; at large enough Reynolds numbers, turbulent drag reduction speeds up the flow, but at the late stage, the slightly increased viscosity brakes stronger than in the case of clean water. Based on the crossover value of d_0 , we can define another percent drag reduction, $DR_{d_0}(\%) = (d_{0,cw} - d_0)/d_{0,cw}$, which is approximately 26% in our case.

The other possible measure, $\Delta x(t)$, is plotted for two fixed instants as a function of the filling height in Fig. 12. Two different methods are used to obtain the data. One is the simple equal time difference shown in Fig. 5a. The other takes into account that the function $\Delta x(t)$ tends to decrease after saturation, therefore, the maximum values are also plotted (empty circles), irrespective of the time of occurrence. Figure 12 shows that the difference is not too large. Extrapolation in Fig. 12a suggests that drag reduction does indeed disappear below a critical filling height, $d_{0c} \approx 9$ cm. This is consistent with the existence of an onset Reynolds number, Re_{dr} .

Similarly to Fig. 10b, Fig. 12b demonstrates the diminishing character of the drag reduction effect in shallow ambient layers.

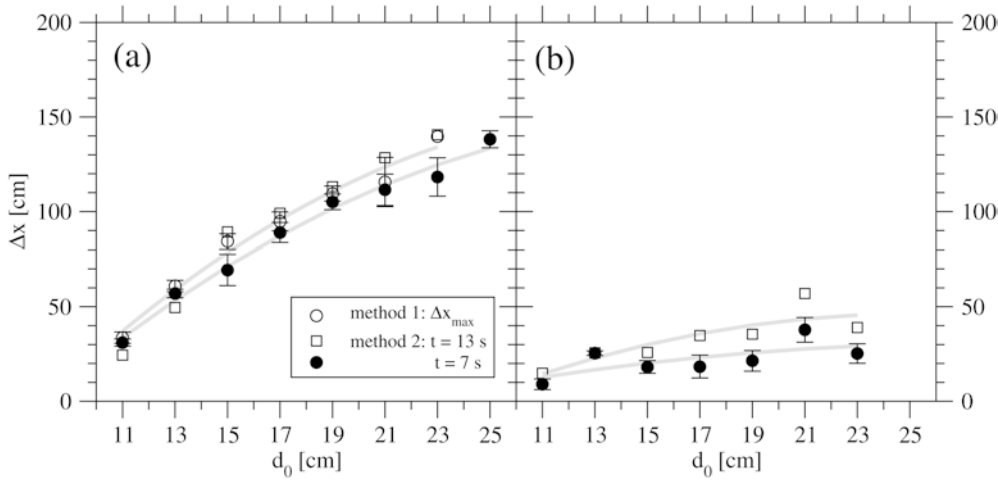


Fig. 12. Displacement difference, Δx , as a function of release height, d_0 , for (a) dry bed runs and (b) in a layer of $d=5$ mm (PEO concentration=42 wppm). Empty circles: maximum difference; empty squares and filled circles: equal time difference (see Fig. 5a) at 7 s and 13 s

3.6 Empirical scaling

The results of the previous subsection suggest that it is worth checking self-similarity from the point of view of the filling height in the lock, since every quantity observed changes monotonously and smoothly as a function of d_0 . We found that a simple rescaling of the spatial variable as $x \rightarrow xd_0^{-\alpha}$ results in quite a good data collapse (see Fig. 13).

Figure 13a shows the result for dry bed runs. The data fall onto two “universal” curves, one for the clean water experiments (empty symbols), the other for the PEO additive ($c=42$ wppm). There should be a gradual transition between the two master curves because there is no drag reduction at low Reynolds numbers; that is, the critical filling height, d_{0c} , must be exceeded. Indeed, data for the lowest value ($d_0=11$ cm) clearly lie between the two curves.

Data for the shallow ambient layer runs seem to also collapse onto a universal curve (Fig. 13b). However, the separation for the clean and PEO polluted water is not clear, which is consistent with the previous observations.

Acceptable data collapse was obtained in the range $\alpha=[0.45, 0.55]$ for both sets in Fig. 13. It is tempting to conclude that the scale exponent is 1/2, whereas we find further differences when considering the time-dependence as well. Straight lines on a double logarithmic plot indicate different power law behavior for the flows over a dry bed and over an ambient fluid layer. The latter seems to be analogous with the classical gravity currents; the slopes are close to the values expected from other experiments (Simpson 1997). As for the dry bed runs, the initial slope is definitely less than 1; it is closer to 4/5, as illustrated in Fig. 13a. On the other hand, a power law with an exponent value of 4/5 does not seem to fit to the curves of the finite ambient layer runs anywhere; see the dashed line in Fig. 13b.

The empirical findings above do not seem to fit to any theoretical scaling relationship known to us. Notwithstanding, we recall two scaling relationships for the inertial and viscous flow regimes, following Huppert (1982). When inertial forces balance gravitational driving, the front of a finite volume fluid evolves as

$$x(t) \sim (gx_0 d_0)^{1/3} t^{2/3}. \quad (2)$$

In the case of a viscous balance, a different scaling holds:

$$x(t) \sim \left(\frac{gx_0^3 d_0^3}{\nu} \right)^{1/5} t^{1/5}. \quad (3)$$

The second approximation is only valid at low Reynolds numbers, i.e., very close to the standstill of spreading. Comparing the empirical slopes, we can observe that the late stage behavior of the front over a finite ambient fluid is close to an inertial gravity current, which also predicts scaling with $d_0^{1/3}$. Dry bed runs, however, seem to deviate from the inertial behavior, although they are certainly not low Reynolds number viscous flows. Nevertheless, a viscous current would scale with $d_0^{0.6}$ according to the prediction.

The important point above is that the role of friction is completely different at dry bed flows. Inevitably, we should not expect a unique scaling exponent for the initial filling height.

4 Discussion

It is known that turbulent drag reduction is strongly connected with skin friction, as it is a surface phenomenon (Gyr and Bewersdorff 1995). However, if we compare a dry bed experiment with a shallow ambient layer run, it is not obvious why drag reduction is not effective in the latter case; the potential energy released is the same, the velocity of front propagation is almost the same (see Fig. 3) and, furthermore, dry bed flows seem to be much less turbulent.

Interesting details are revealed by the sequence of Fig. 14, where clean water was released into the channel containing a colored ambient fluid layer. Flow from the lock always departs at the bottom, since the hydrostatic pressure is largest there. On the other hand, the resting fluid in the channel tends to block the flow, the collision with the moving front results in an upthrust generating the “mushroom” jet (see Fig. 14). An essential point is that the fluid volume starting from the lock does not spread over the channel; its kinetic energy is

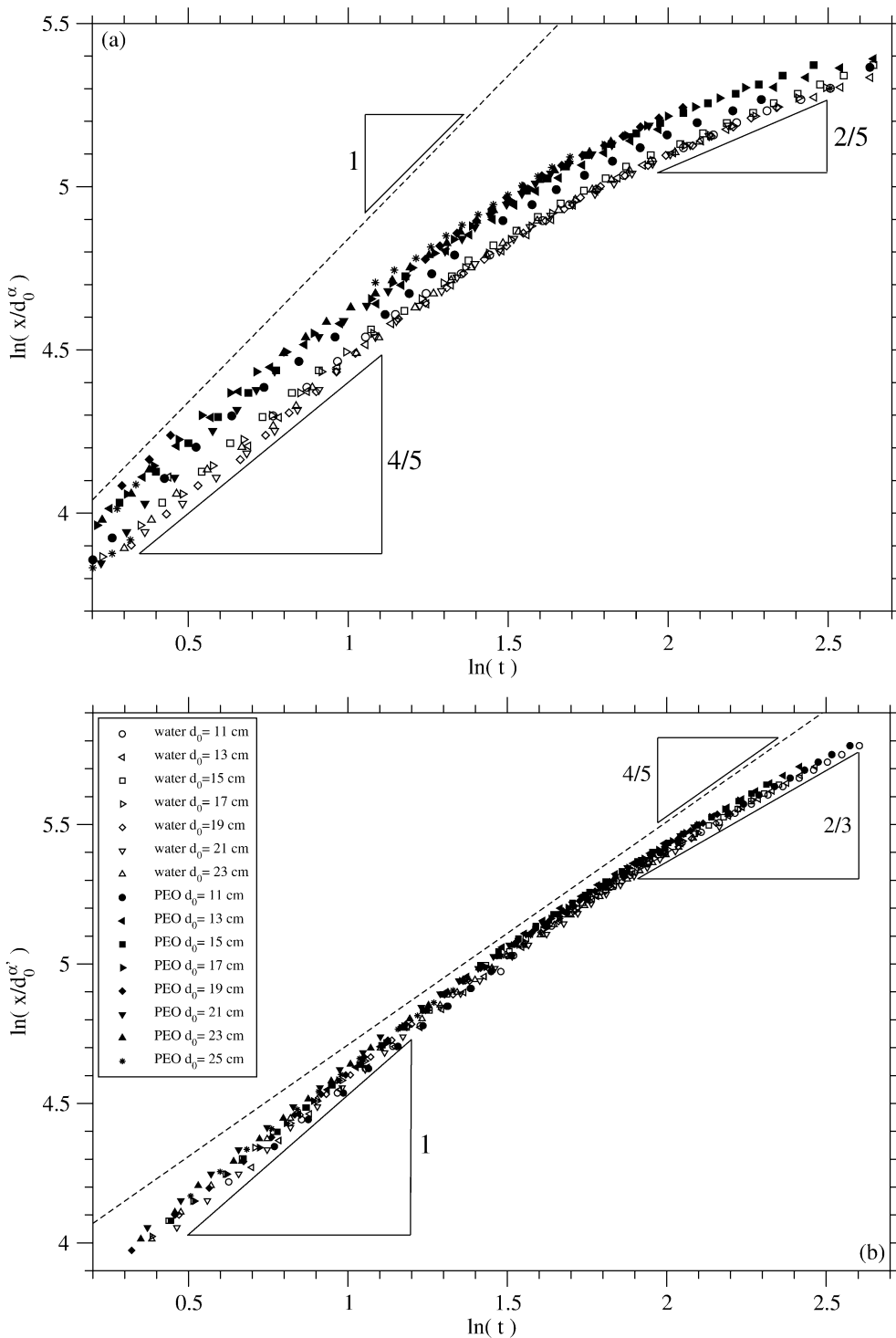


Fig. 13a, b. Scaled values, x/d_0^α , of the front displacements as a function of time for both pure water and PEO solutions (concentration 42 wppm). All of the data belonging to different release heights, d_0 , fall on a master curve with $\alpha=0.55$ for (a) the dry bed case and (b) with $\alpha=0.45$ for the shallow ambient layer case ($d=5$ mm). The slope of the dashed line is 1 in a and 4/5 in b. Note the double-logarithmic scale

transferred to water parcels resting in the channel at the beginning. The higher the fluid level in the channel, d , the smaller the displacement of the water volume from the lock (see Fig. 15).

This observation cannot fully explain the lack of drag reduction at shallow ambient layer depths because the fluid in the channel contains dissolved PEO at the same concentration as in the lock. It is plausible to assume that drag reduction is most effective at the early stages of the flow, where the flow speed is the largest and, thus, the turbulence is most vigorous. The results support the

conjecture that the type of turbulence does matter (Cadot et al. 1998); drag reduction is more efficient when the turbulence is homogeneous (smooth boundary layer excitation) and less efficient when it is strongly heterogeneous with wave breaking, bubbling, foaming, etc. (inertial excitation).

Let us return shortly to the problem of defining percentage drag reduction (DR%) for our experiments. As we explained, a sole number can not easily characterize the effect of PEO because dam-break flow with a small reservoir is essentially a transient phenomenon.

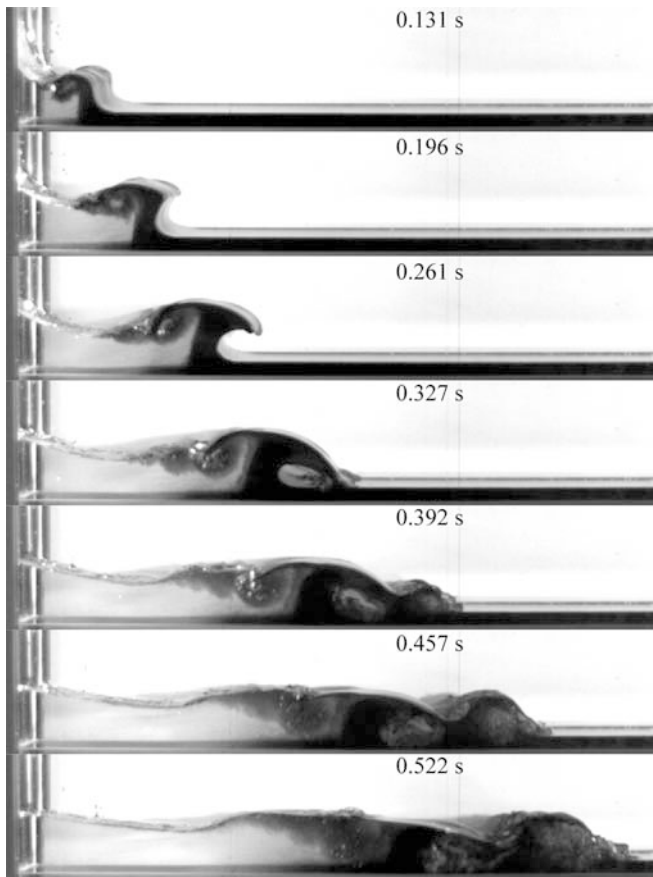


Fig. 14. Release of a dam-break front into a colored ambient water layer of $d=15$ mm. The transparent fluid pushes up the dark layer so much that practically none of it remains behind the front. A mushroom-like object is formed on the free surface leading to a partial mixing in its wake. The role of the transparent fluid is mainly to bring into motion the ambient water layer. This explains the very weak drag reduction effect in this case

The main points of our observation can be summarized as follows:

1. Many characteristics of dam-break flow depend strongly on whether the front propagates on a dry channel bed or over an ambient fluid layer. For dry bed runs, the initial flow is much faster but later, the frictional braking is stronger (Fig. 3). The vertical cross-section of the flow in a dry channel is smooth (Fig. 2), while a front over a fluid layer generates unstable jets, wave breaking, bubble trapping, etc. (Fig. 2).
2. Turbulent drag reduction works only for dry bed experiments. The effect of PEO is almost negligible whenever a thin ambient layer is present (Figs. 5, 10, 12, 13).
3. The dam-break flow provides an example of a free surface flow. The textural change of the surface due to the presence of PEO is remarkable; elongated structures become visible (Fig. 6). It is tempting to speculate that they are fingerprints of the coherent structures characterizing the flow close to the wall (Nagata 1990; Clever and Busse 1992, 1997; Schmiegel and Eckhardt 1997, 2000; Eckhardt et al. 2002; Stone and Graham 2003) whose relative strength might be influenced by the

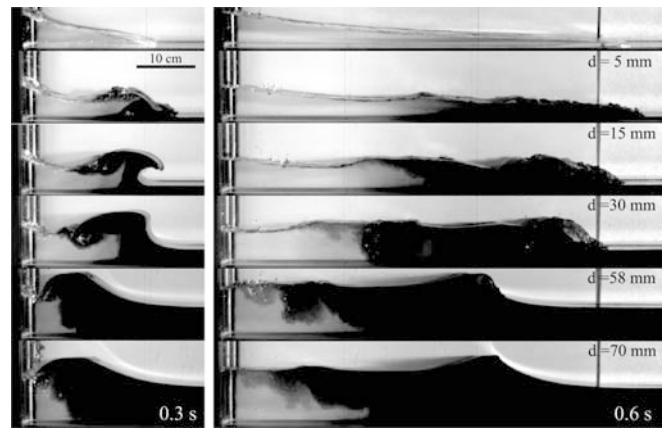


Fig. 15. Release of a dam-break front into a colored ambient water layer of increasing depth, d (from top to bottom). The filling height was $d_0=15$ cm in each case. Elapsed time at the left and right columns is $t=0.3$ and 0.6 s, respectively

polymer concentration (De Angelis et al. 2003). A further detailed investigation of this phenomenon is necessary.

References

- Benzi R, Ching ESC, Horesh N, Procaccia I (2004) Theory of concentration dependence in drag reduction by polymers and of the maximum drag reduction asymptote. *Phys Rev Lett* 92:078302
- Berman NS (1978) Drag reduction by polymers. *Annu Rev Fluid Mech* 10:47–64
- Boffetta G, Celani A, Musacchio S (2003a) Two-dimensional turbulence of dilute polymer solutions. DOI 10.1103/PhysRevLett.91.034501
- Boffetta G, Celani A, Mazzino A (2003b) Onset and universality of drag reduction in turbulent Kolmogorov flow. lanl.arXiv.org/nlin-0309036
- Brannan DA, Esplen M, Gray J (1999) *Geometry*. Cambridge University Press, Cambridge
- Bushnell DM (1991) Drag reduction in nature. *Annu Rev Fluid Mech* 23:65–79
- Cadot O, Bonn D, Douady S (1998) Turbulent drag reduction in a closed flow system: Boundary layer vs bulk effects. *Phys Fluids* 10:426–436
- Clever RM, Busse FH (1992) Three-dimensional convection in a horizontal fluid layer subjected to a constant shear. *J Fluid Mech* 234:511–527
- Clever RM, Busse FH (1997) Tertiary and quaternary solutions for plane Couette flow. *J Fluid Mech* 344:137–153
- De Angelis E, Casciola CM, L'vov VS, Piva R (2003) Drag reduction by polymers in turbulent channel flows: Energy redistribution between invariant empirical modes. DOI 10.1103/PhysRevE.67.056312
- Eckhardt B, Faisst H, Schmiegel A, Schumacher J (2002) Turbulence transition in shear flows. In: Castro IP, Hancock PE, Thomas TG (eds) *Advances in Turbulence IX*, proceedings of the 9th European turbulence conference, CIMNE, Barcelona, Spain, 2002, pp 1–8
- Gampert B, Wagner P (1985) The influence of molecular weight and molecular weight distribution on drag reduction and mechanical degradation in turbulent flow of highly dilute polymer solutions. In: Gampert D (ed) *Proceedings of the IUTAM symposium on the influence of polymer additives on velocity and temperature fields*, Essen, Germany, June 1984, pp 71–85
- Gröbelbauer HP, Fanneløp TK, Britter RE (1993) The propagation of intrusion fronts of high density ratios. *J Fluid Mech* 250:669–687
- Gyr A, Bewersdorff HW (1995) *Drag reduction of turbulent flows by additives*. Kluwer Academic Publ, Dordrecht

- Housiadas KD, Beris AN (2003) Polymer-induced drag reduction: Effects of the variations in elasticity and inertia in turbulent viscoelastic channel flow. *Phys Fluids* 15:2369–2384
- Huppert HE (1982) The propagation of two dimensional and axisymmetric viscous gravity currents over a rigid horizontal surface. *J Fluid Mech* 121:43–58
- Klemp JB, Rotunno R, Skamarock WC (1997) On the propagation of internal bores. *J Fluid Mech* 331:81–106
- Kondic L (2003) Instabilities in gravity driven flow of thin fluid films. *SIAM Rev* 45:95–113
- L'vov VS, Pomyalov A, Procaccia I, Tiberkevich V (2003) Drag reduction by polymers in wall bounded turbulence. [lanl.arxiv.org:nlin-0307034](http://lanl.arxiv.org/nlin-0307034)
- Lumley JL (1969) Drag reduction by additives. *Annu Rev Fluid Mech* 1:367–384
- Min T, Yoo JY, Choi H, Joseph DD (2003a) Drag reduction by polymer additives in a turbulent channel flow. *J Fluid Mech* 486:213–238
- Min T, Choi H, Yoo JY (2003b) Maximum drag reduction in a turbulent channel flow by polymer additives. *J Fluid Mech* 492:91–100
- Nagata M (1990) Three-dimensional finite-amplitude solutions in plane Couette flow: Bifurcation from infinity. *J Fluid Mech* 217:519–527
- Paireau O, Bonn D (1999) Drag reduction in liquid-liquid friction. *Phys Rev Lett* 83:5591–5594
- Ptasinski PK, Boersma BJ, Nieuwstadt FTM, Hulsen MA, Van den Brule BHAA, Hunt JCR (2003) Turbulent channel flow near maximum drag reduction: simulations, experiments and mechanisms. *J Fluid Mech* 490:251–191
- Ritter A (1892) Die Fortpflanzung der Wasserwellen. *Zeitschrift des Vereines Deutscher Ingenieure* 36:947–954
- Schmiegel A, Eckhardt B (1997) Fractal stability border in plane Couette flow. *Phys Rev Lett* 79:5250–5253
- Schmiegel A, Eckhardt B (2000) Persistent turbulence in annealed plane Couette flow. *Europhys Lett* 51:395–400
- Simpson JE (1997) Gravity currents: In the environment and laboratory. Cambridge University Press, Cambridge
- Sreenivasan KR, White CM (2000) The onset of drag reduction by dilute polymer additives, and the maximum drag reduction asymptote. *J Fluid Mech* 409:149–164
- Stansby PK, Chegini A, Barnes TCD (1998) The initial stages of dam-break flow. *J Fluid Mech* 374:407–424
- Stone PA, Waleffe F, Graham MD (2002) Toward a structural understanding of turbulent drag reduction: Nonlinear coherent states in viscoelastic shear flows. *Phys Rev Lett* 89:208301–1-4
- Stone PA, Graham MD (2003) Polymer dynamics in a model of the turbulent buffer layer. *Phys Fluids* 15:1247–1256
- Sturm TW (2001) Open channel hydraulics. McGraw-Hill Science, New York
- Toms BA (1949) Observation on the flow of linear polymer solutions through straight tubes at large Reynolds numbers. In: Proceedings of the international rheological congress, Amsterdam, North Holland, II-135–141
- Virk PS (1975) Drag reduction fundamentals. *AIChE J* 21:625–656